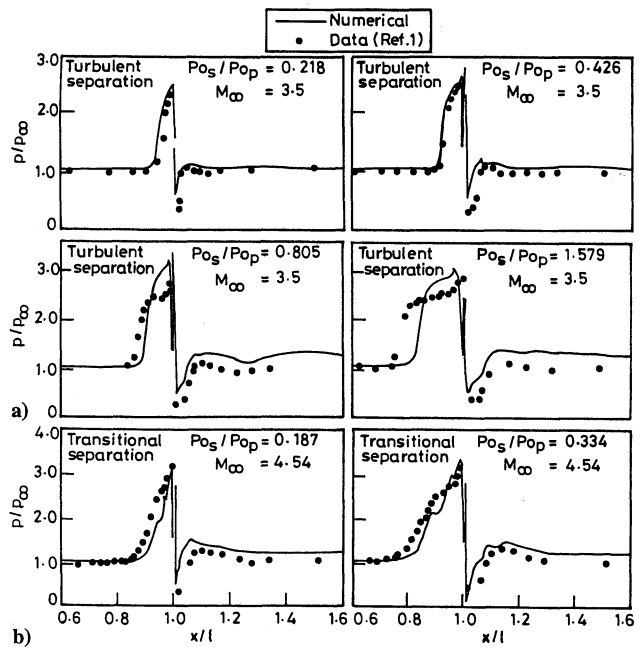

Fig. 3 Comparison of predicted and measured surface static pressures for a) turbulent and b) transitional separations.

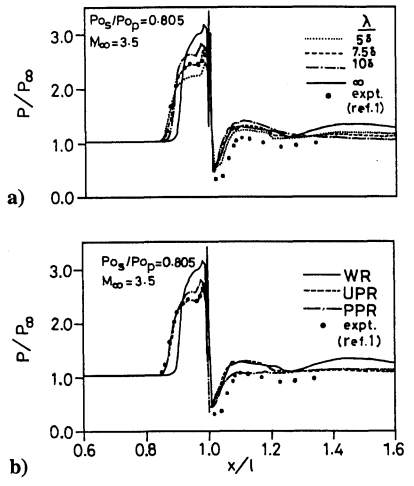

Fig. 4 Surface static pressure distributions depicting a) the effect of relaxation length and b) the performance of the two relaxation models.

rise found in the turbulent separation cases. Upstream pressures are underpredicted, whereas downstream pressures are overpredicted. However, the overall trend is very encouraging despite the crude transition model used.

In an attempt to extend the applicability of the BL model for jet interaction flows with large upstream separation, relaxation terms are incorporated in the present study. The values of x_0, the point at which upstream pressure starts increasing, are taken as 0.1886 m for $Po_s/Po_p = 0.805$ and 0.1715 m for $Po_s/Po_p = 1.579$ (from experiments). To apply the model, the relaxation length λ has to be determined first. Figure 4a shows the effect of λ on the surface pressure distribution. The case $\lambda = \infty$ corresponds to the equilibrium model, that is, without relaxation (WR). Decreasing λ increases the upstream pressure propagation and decreases the upstream pressure peak. The optimum λ for this case is found to be $7.5\delta_0$, where δ_0 is the boundary-layer thickness at x_0 (Fig. 4a). For the case with $Po_s/Po_p = 0.805$, both models predict the same upstream separation location (Fig. 4b). Though the PPR model overpredicts the upstream pressure peak slightly, it is excellent in the downstream pressure prediction. For the highest pressure ratio case ($Po_s/Po_p = 1.579$), the PPR model underpredicts the upstream pressure propagation although there is some improvement when compared to the equilibrium model (WR). The UPR model predicts the upstream pressure distribution well and, therefore, gives a better overall prediction. In general, significant improvement is observed in the predictions with the incorporation of relaxation terms.

Conclusions

Jet interaction flowfields with turbulent and transitional separation for a wide range of freestream to injectant total pressure ratios are simulated numerically. Calculations with the BL model show reasonably accurate results, in general, except for flows with large injectant-to-freestream-total-pressure ratios attended by large upstream separation, where it underpredicts the upstream separation and overpredicts the upstream peak pressure. With the inclusion of relaxation terms in the BL model, significant improvement in terms of better upstream pressure propagation and reduced peak pressure over those without relaxation are obtained. Of the two relaxation models used, the UPR model performs better. In the case of transitional separation, qualitative agreement is observed, despite the crude transition model employed.

References

[1]Spaid, F. W., and Zukoski, E. E., "A Study of the Interaction of Gaseous Jets from Transverse Slots with Supersonic External Flows," *AIAA Journal*, Vol. 6, No. 2, 1968, pp. 205–212.

[2]Baldwin, B., and Lomax, H., "Thin Layer Approximation and Algebraic Model for Separated Turbulent Flows," AIAA Paper 78-257, 1978.

[3]Hung, C. M., "Development of Relaxation Turbulence Models," NASA CR-2783, Dec. 1976.

[4]Hung, C. M., and MacCormack, R. W., "Numerical Solutions of Supersonic and Hypersonic Laminar Compression Corner Flows," *AIAA Journal*, Vol. 14, No. 4, 1976, pp. 475–481.

[5]Harten, A., and Zwas, G., "Switched Numerical Shumann Filters for Shock Calculations," *Journal of Engineering Mathematics*, Vol. 6, No. 2, 1972, pp. 207–216.

F. W. Chambers
Associate Editor

Mach Reflection Wave Configuration in Two-Dimensional Supersonic Jets of Overexpanded Nozzles

H. Li* and G. Ben-Dor†
Ben-Gurion University of the Negev, Beer-Sheva 84105, Israel

Introduction

A CONVERGING/DIVERGING nozzle is a device by which supersonic flows can be produced. Applications of such flows are supersonic wind tunnels, rocket nozzles, gas lasers, etc. An excellent and comprehensive discussion of the possible flows through such nozzles is given in Ref. 1. The ambient pressure P_∞ is the key parameter in determining the nature of the flow in the nozzle and the jet emanating from it. When the exit flow is supersonic, the exit plane pressure P_3 may be larger, equal, or smaller than P_∞. When $P_3 < P_\infty$, the nozzle is overexpanded and two oblique shock waves are formed at the lips of the nozzle (Fig. 1a). The interaction of these oblique shock waves results in either a regular or a Mach reflection (Fig. 1a). In overexpanded nozzles, an analytical solution exists only when the resulting wave configuration is a regular reflection. An analytical solution for situations in which the

Received Feb. 14, 1996; accepted for publication Nov. 29, 1997.

*Postdoctoral Fellow, Department of Mechanical Engineering.

†Professor, Dean of the Faculty of Engineering Sciences, Pearlstone Center for Aeronautical Engineering Studies, Department of Mechanical Engineering.

resulting wave configuration is a Mach reflection is not available because such a solution requires a model for predicting the Mach stem height. However, such models were advanced only recently.[2,3] The aim of the present study is to present an analytical solution of the case of an overexpanded nozzle flow with a Mach reflection, which is different from that proposed in Refs. 2 and 3.

Present Study

The following analysis is restricted to two-dimensional flows. Because the flow is symmetric, only the part on one side of the symmetry line will be solved. A scheme of the flowfield to be solved together with the definition of relevant parameters is shown in Fig. 1b. The wave configuration consists of three parts, a Mach reflection with triple point T, an interaction of the reflected shock wave r with the jet boundary at point A, which results in a centered Prandtl–Meyer expansion fan, and the interaction of this expansion fan with the slipstream s.

The solution of the flowfield requires a model by which the distance from the triple point T to the symmetry line (H_m in Fig. 1b) can be calculated. The basic idea of the present model, developed in the course of this study, was originally proposed by Ref. 2. It was assumed that the slipstream s and the line of symmetry form a one-dimensional converging nozzle inside which the flow is isentropic and that the throat is located at the point where the head of the expansion fan intersects the slipstream (point B in Fig. 1b). The latter assumption was found to be incorrect.[3] Instead, Ref. 3 assumed that, as a result of the interaction with the expansion fan, the slipstream assumes the shape of a second-order polynomial, which extends from point B to point E in Fig. 1b. In addition, whereas Refs. 2 and 3 assumed that the Mach stem m is straight and perpendicular to the symmetry line, the present analysis allows the Mach stem to be curved. Hence, the flow immediately behind it is not necessarily uniform.

In addition, it has been assumed that the gas is perfect, the fluid is ideal, the reflection of the centered expansion fan from the slipstream is neglected, the flow in region 4 is supersonic, the two slipstreams form a two-dimensional converging/diverging nozzle, and the flow in the throat is sonic and is supersonic downstream of it.

The three-shock theory[4] can be used to solve the flowfield associated with the triple point T. Let us define the states ahead of and behind an oblique shock wave as i and j, respectively. The conservation equations relating states i and j are

$$\rho_i u_i \sin\phi_j = \rho_j u_j \sin(\phi_j - \theta_j) \tag{1}$$

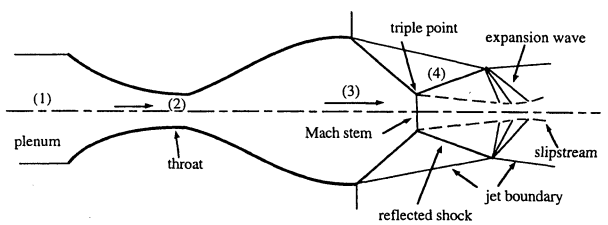

Fig. 1a Scheme of the overexpanded flow with a Mach reflection.

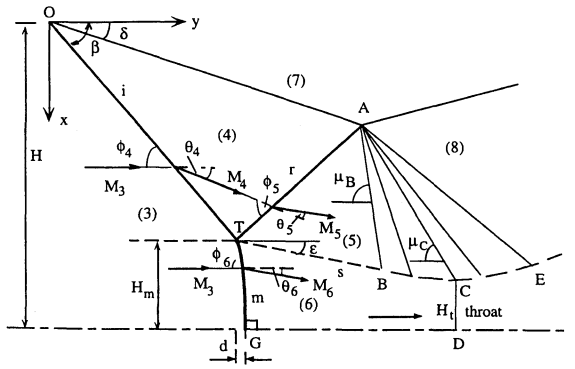

Fig. 1b Scheme and definition of parameters of the wave system associated with a Mach reflection.

$$P_i + \rho_i u_i^2 \sin^2\phi_j = P_j + \rho_j u_j^2 \sin^2(\phi_j - \theta_j) \tag{2}$$

$$\rho_i \tan\phi_j = \rho_j \tan(\phi_j - \theta_j) \tag{3}$$

$$[\gamma/(\gamma-1)](P_i/\rho_i) + \tfrac{1}{2}u_i^2 \sin^2\phi_j = [\gamma/(\gamma-1)](P_j/\rho_j) + \tfrac{1}{2}u_j^2 \sin^2(\phi_j - \theta_j) \tag{4}$$

where u [$u = Ma$, M is the flow Mach number, and $a = (\gamma P/\rho)^{1/2}$ is the sound speed] is the flow velocity, P the pressure, ρ the density, and γ the specific heat ratio. For the incident shock i, $i = 3$ and $j = 4$; for the reflected shock r, $i = 4$ and $j = 5$; and for the Mach stem m near the triple point, $i = 3$ and $j = 6$.

The matching conditions across the jet boundary and the slipstream are

$$P_4 = P_7 = P_\infty, \qquad \delta = \theta_4, \qquad \beta = \phi_4$$
$$\theta_4 - \theta_5 = \theta_6, \qquad P_5 = P_6, \qquad \theta_6 = \varepsilon \tag{5}$$

The preceding set of equations consists of 18 equations with 18 unknowns, namely, u_4, u_5, u_6, ρ_4, ρ_5, ρ_6, P_4, P_5, P_6, ϕ_4, ϕ_5, ϕ_6, θ_4, θ_5, θ_6, δ, β, and ε, provided the parameters u_3 ($= M_3 a_3$), P_3, ρ_3, and P_∞ are known. Thus, the set of equations is complete.

Generally, $\varepsilon \neq 0$ and, hence, the Mach stem is usually curved. At its foot (point G in Fig. 1b) it is normal to the upstream flow u_3. Consequently, the normal shock relations are valid at point G. Using the classic normal shock relations,[4] one can easily obtain u_G, ρ_G, and P_G.

The shape of the curved Mach stem is determined by the subsonic flow region behind it. Theoretically, it is impossible to get an exact analytical expression of its shape. However, based on the experiment, it is only slightly curved. Thus, it is reasonable to assume that the shape of the Mach stem can be expressed by a second-order polynomial. Together with the appropriate boundary conditions at points T and G, one finally obtains

$$y = -1/2 \cot\phi_6 (x - H)^2/H_m + (H - H_m)\cot\beta + 1/2 H_m \cot\phi_6 \tag{6}$$

in which H_m, the distance from the triple point to the symmetry line, is an unknown. The horizontal shift of the foot of the Mach stem is

$$d = y_G - y_T = 1/2 H_m \cot\phi_6 \tag{7}$$

The interaction of the centered expansion fan with the slipstream is also shown schematically in Fig. 1b. The flow region ABC can be treated as a simple wave region. In addition, because at the throat the flows on both sides of the slipstream are parallel to the symmetry line, one can write

$$\nu(M_c) - \nu(M_5) = \varepsilon \tag{8}$$

where M_C is flow Mach number along the characteristic AC and $\nu(M)$ the Prandtl–Meyer function.[1] The (x, y) coordinates of points A, B, and C can be expressed as

$$x_A = (H - H_m)[\cot\beta + \cot(\phi_5 - \delta)]/[\cot\delta + \cot(\phi_5 - \delta)] \tag{9a}$$

$$y_A = x_A \cot\delta \tag{9b}$$

$$x_B = \frac{H - H_m}{\cot\varepsilon - \cot(\mu_B + \varepsilon)}\left\{\cot\varepsilon - \cot\beta + \frac{[\cot\delta - \cot(\mu_B + \varepsilon)][\cot\beta + \cot(\phi_5 - \delta)]}{\cot\delta + \cot(\phi_5 - \delta)}\right\} \tag{10a}$$

$$y_B = [x_B - (H - H_m)]\cot\varepsilon + (H - H_m)\cot\beta \tag{10b}$$

$$x_C = H - H_t \tag{11a}$$

$$y_C = (H - H_t)\cot\mu_C + x_A(\cot\delta - \cot\mu_C) \tag{11b}$$

where $\mu_B = \arcsin(1/M_5)$, $\mu_C = \arcsin(1/M_C)$, and H_t is the height of sonic throat (Fig. 1b).

Under the first-order approximation, the relation between points B and C is

$$x_B - x_C = 1/2(y_B - y_C)\tan\varepsilon \tag{12}$$

Because $|\varepsilon| \ll 1$ it is reasonable to assume that the flow in the duct formed by the slipstream and the symmetry line (TC and GD in Fig. 1b) is quasi-one dimensional. In addition, if it is assumed that the flow at the throat is sonic, the well-known area-Mach number relation is

$$(H_m/H_t) = (1/M)([2/(\gamma+1)]\{1+[(\gamma-1)/2]\bar{M}^2\})^{(\gamma+1)/2(\gamma-1)} \tag{13}$$

Here, $\bar{M} = \bar{u}/\bar{a}$ can be regarded as the average flow Mach number behind the curved Mach stem. Under a first-order approximation, one obtains

$$\bar{M} = \frac{2(\rho_6 u_6 \cos\varepsilon + \rho_G u_G)}{(\rho_6 + \rho_G)(a_6 + a_G)} \tag{14}$$

where $u_6 = M_6 a_6$ and $u_G = M_G a_G$, ρ_6, a_6, M_6, and ε can be found by solving the set of Eqs. (1–5) and M_G, ρ_G, and a_G are given by the normal shock relations.

Combining Eqs. (10–14), one finally obtains the following relations:

$$\frac{H_m}{H} = 1 - \frac{(1-L)(2-\tan\varepsilon\cot\mu_C)}{K+1-2L-\tan\varepsilon[\cot\beta - G(\cot\delta - \cot\mu_C) - L\cot\mu_C]} \tag{15}$$

$$H_t/H = L(H_m/H) \tag{16}$$

where

$$G = [\cot\beta + \cot(\phi_5 - \delta)]/[\cot\delta + \cot(\phi_5 - \delta)] \tag{17a}$$

$$K = \frac{1}{\cot\varepsilon - \cot(\mu_B + \varepsilon)}\left\{\cot\varepsilon - \cot\beta + \frac{[\cot\delta - \cot(\mu_B+\varepsilon)][\cot\beta + \cot(\phi_5 - \delta)]}{\cot\delta + \cot(\phi_5 - \delta)}\right\} \tag{17b}$$

$$L = \bar{M}([2/(\gamma+1)]\{1+[(\gamma-1)/2]\bar{M}^2\})^{-(\gamma+1)/2(\gamma-1)} \tag{17c}$$

Equations (15–17) give the values of H_m and H_t provided the rest of the parameters are known. Actually, H_m/H and H_t/H depend only on the values of M_3 and P_3/P_∞.

Results and Discussion

The nondimensional Mach stem height H_m/H vs the pressure ratio P_3/P_∞ is shown in Fig. 2a for different oncoming flow Mach numbers M_3. When H_m/H becomes zero, the Mach reflection terminates and a regular reflection is formed. The dependence of H_m/H on M_4 is shown in Fig. 2b. It is evident that, when $M_4 = 1$, $H_m/H = 1$, i.e., the Mach stem stands exactly at the exit plane of the nozzle, in full agreement with Ref. 1 (p. 101). The dependence of the nondimensional throat height H_t/H on the pressure ratio P_3/P_∞ is shown in Fig. 2c. Knowing the value of H_t enables one to predict the cell size of the wave pattern that results from the jet outside the nozzle. Figure 2d shows the dependence of the nondimensional maximum horizontal shift of the curved Mach stem d/H_m on the pressure ratio P_3/P_∞. The maximum value of d/H_m for $M_3 = 5$ and $\gamma = 1.4$ does not exceed 0.1. Hence, the Mach stem can be approximately assumed to be straight.

Because of the lack of experimental data for two-dimensional nozzle flows for comparison with analytical predictions, available numerical results were used to verify the present developed model. Numerical simulations using different schemes for wedge-generated Mach reflection wave configurations in steady flows were presented in Refs. 4 and 5. When the reflected shock wave touches the trailing edge of the reflecting wedge, the resulting wave configurations are qualitatively identical to that modeled in the present study and, hence, can be solved by the presently derived governing equations. Figure 2e (Refs. 5 and 6) shows the dependence of the Mach stem height H_m/H on the incident shock wave angle β. The fact that two numerical data points are located close to the present analytical line suggests that the developed model is reasonable. Finally, an analytically predicted wave configuration associated with a Mach reflection outside the two-dimensional supersonic jet of an overexpanded nozzle is shown in Fig. 3.

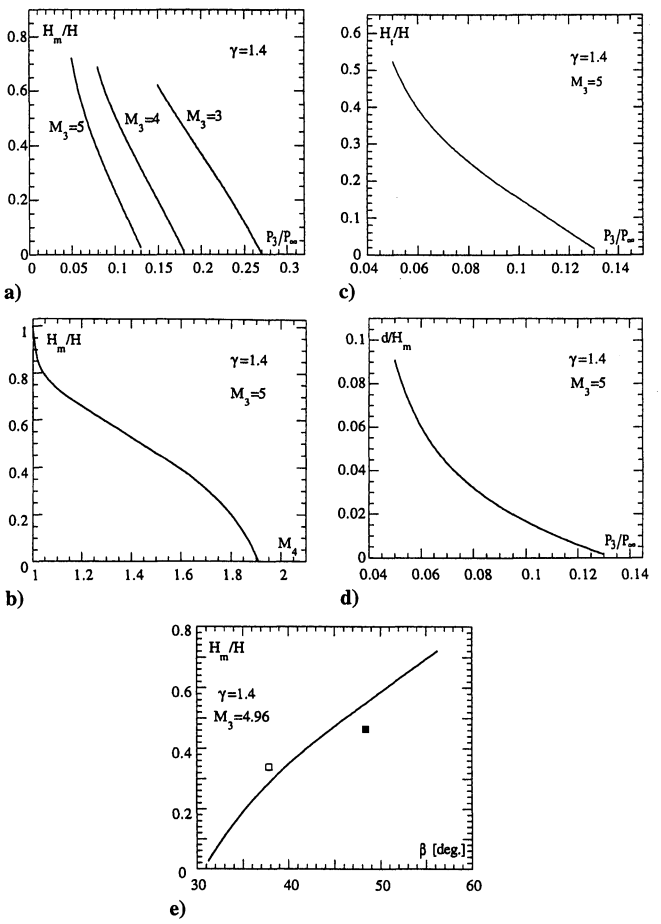

Fig. 2 Dependence of the nondimensional Mach stem height H_m/H a) on the pressure ratio P_3/P_∞ for different oncoming flow Mach numbers M_3 and b) on the flow Mach number in region 4, M_4; c) dependence of the nondimensional throat height H_t/H on the pressure ratio P_3/P_∞; d) dependence of the nondimensional maximum horizontal shift of the foot of the curved Mach stem d/H_m on the pressure ratio P_3/P_∞; and e) dependence of the nondimensional Mach stem height H_m/H on the incident shock wave angle β; solid[5] and open[6] squares are numerical results.

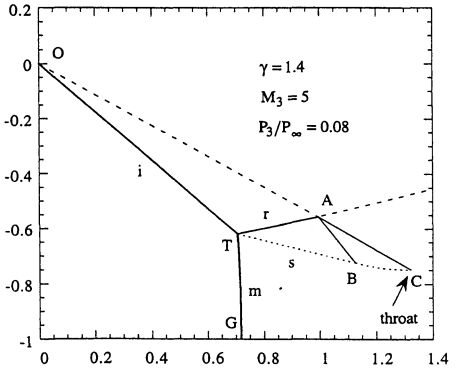

Fig. 3 Analytical prediction of the wave configuration associated with a Mach reflection outside the two-dimensional supersonic jet of an overexpanded nozzle.

Conclusion

The Mach reflection wave configurations and the flowfields associated with two-dimensional supersonic free jets of overexpanded nozzles were analyzed. Based on the two- and the three-shock theories along with the classical gasdynamics theory, an analytical model for calculating the height of Mach stem and the cell size of the jet was proposed. Comparison with numerical calculations suggested that the present developed model is reasonable. To the best of the authors' knowledge, the present analytical model is the only available model that is capable of dealing with Mach reflection wave configurations in supersonic jets of overexpanded nozzles.

References

[1]Emanuel, G., "Nozzle and Diffuser Flow," *Gasdynamics: Theory and Applications*, AIAA Education Series, AIAA, New York, 1986, pp. 89–101.

[2]Azevedo, D. J., and Liu, C. S., "Engineering Approach to the Prediction of Shock Patterns in Bounded High-Speed Flows," *AIAA Journal*, Vol. 31, No. 1, 1993, pp. 83–90.

[3]Schotz, M., Levy, A., Ben-Dor, G., and Igra, O., "Analytical Prediction of the Wave Configuration Size in Steady Flow Mach Reflections," *Shock Waves*, Vol. 7, No. 6, 1997, pp. 363–372.

[4]Ben-Dor, G., "Analytical Approaches for Describing Regular and Mach Reflections," *Shock Wave Reflection Phenomena*, Springer, New York, 1991, pp. 10–16.

[5]Chpoun, A., Passerel, D., Lengrand, J. C., Li, H., and Ben-Dor, G., "Mise en Évidence Expérimentale et Numérique d'un Phénoméne d'Hystérésis lors de la Transition Réflexion de Mach-Réflexion Réguliére," *Comptes Rendus à l'Académie des Sciences*, Vol. 319, Ser. 2, Paris, 1994, pp. 1447–1453.

[6]Vuillon, J., Zeitoun, D., and Ben-Dor, G., "Reconsideration of Oblique Shock Wave Reflection in Steady Flows. Part II: Numerical Investigation," *Journal of Fluid Mechanics*, Vol. 301, 1995, pp. 37–50.

D. Parekh
Associate Editor

Direct Updating of Damping and Stiffness Matrices

M. I. Friswell*
University of Wales,
Swansea SA2 8PP, Wales, United Kingdom
and
D. J. Inman† and D. F. Pilkey‡
Virginia Polytechnic Institute and State University,
Blacksburg, Virginia 24061-0219

Introduction

MODEL updating is becoming a common method to improve the correlation between finite element models and measured data.[1,2] A number of approaches to the problem exist, based on the type of parameters that are updated and the measured data that are used. This Note concentrates on a direct updating method based on measured modal data. These methods update complete structural matrices, so that the updated matrices are those closest to the initial analytical matrices but reproduce the measured data. For example, Baruch[3,4] considered the mass matrix to be exact and updated the stiffness matrix. A preliminary step estimated the mass normalized eigenvectors closest to the measured eigenvectors. Berman[5,6] questioned whether the mass matrix should be considered exact and updated both the mass matrix and the stiffness matrix. Baruch[7] described these methods as reference basis methods because one of three quantities (the measured modal data and the analytical mass and stiffness matrices) is assumed to be exact, or the reference, and the other two are updated. Caesar[8] extended this approach and produced a range of methods based on optimizing a number of cost functions. All of the methods described thus far share the feature that only one quantity is updated at a time. Wei[9–11] updated the mass and stiffness matrices simultaneously, using the measured modal data as a reference. The constraints imposed were mass orthogonality, the equation of motion, and the symmetry of the updated matrices.

All of the methods described used real mode shapes and natural frequencies. The measured mode shapes were processed to produce the equivalent real modes. This Note extends the reference basis methods by updating the damping matrix. Fuh et al.[12] proposed a method that updates the mass and damping matrices with the constraint of orthogonality. The stiffness matrix is then updated to ensure the measured modal model is reproduced. Weighted norms between the initial and updated mass, damping, and stiffness matrices are minimized. In this Note, the mass matrix is assumed correct and the damping and stiffness matrices are updated simultaneously, so that the updated model reproduces the measured modal data.

Updating Method

Following the method of Baruch,[3,4] who updated the stiffness matrix only, the difference between the initial and updated damping and stiffness matrices is minimized, with the constraints that the eigenvalue equation is satisfied and that the damping and stiffness matrices are symmetric (and, of course, real). Thus, the penalty function to be minimized is given by

$$J = \tfrac{1}{2}\left\|\boldsymbol{N}^{-1}[\boldsymbol{K}-\boldsymbol{K}_a]\boldsymbol{N}^{-1}\right\|^2 + \tfrac{1}{2}\mu\left\|\boldsymbol{N}^{-1}[\boldsymbol{C}-\boldsymbol{C}_a]\boldsymbol{N}^{-1}\right\|^2 \quad (1)$$

subject to

$$\boldsymbol{M}_a\Phi\Lambda^2 + \boldsymbol{C}\Phi\Lambda + \boldsymbol{K}\Phi = \boldsymbol{0} \quad (2)$$

$$\boldsymbol{C} = \boldsymbol{C}^T, \qquad \boldsymbol{K} = \boldsymbol{K}^T \quad (3)$$

where $\boldsymbol{N}=\boldsymbol{M}_a^{1/2}$; $\boldsymbol{M}_a$, $\boldsymbol{C}_a$, and $\boldsymbol{K}_a$ are the initial, analytical mass, damping, and stiffness matrices; $\boldsymbol{C}$ and $\boldsymbol{K}$ are the updated damping and stiffness matrices; and Φ and Λ are the measured eigenvector and eigenvalue matrices. The extension for other weighting matrices $\boldsymbol{N}$ and, indeed, for different weighting of the damping and stiffness matrices is straightforward. A full set of modes is not measured, so that Φ is not square, but all degrees of freedom (DOFs) are assumed measured. If only a subset of the DOFs is measured, then the model must be reduced or the mode shapes expanded. Λ is a diagonal matrix with the measured eigenvalues on the diagonal. The parameter μ in Eq. (1) is to enable the damping and stiffness terms to be weighted. Often the magnitude of the stiffness terms is far greater than that of the damping terms, and so if μ were not present more weight would be given to the stiffness terms, leading to a poor estimate of the damping matrix. The value of μ is selected based on experience, often using the results from a range of values. This will be discussed further in the example. Note that Wei[9–11] produced a similar method for updating mass and stiffness matrices simultaneously, although he did not include a weighting factor similar to μ. Including such a factor does mean that closed-form solutions for the updated matrices are unlikely, but in practice including this weighting is vital.

The Lagrange multiplier method will now be used to solve the optimization problem. The augmented penalty function based on Eq. (1) and the constraints is

$$\begin{aligned} J = {} & \frac{1}{2}\left\|\boldsymbol{N}^{-1}[\boldsymbol{K}-\boldsymbol{K}_a]\boldsymbol{N}^{-1}\right\|^2 + \frac{1}{2}\mu\left\|\boldsymbol{N}^{-1}[\boldsymbol{C}-\boldsymbol{C}_a]\boldsymbol{N}^{-1}\right\|^2 \\ & + \sum_{i,j=1}^{n}\gamma_{Kij}(k_{ij}-k_{ji}) + \sum_{i,j=1}^{n}\gamma_{Cij}(c_{ij}-c_{ji}) \\ & + 2\sum_{i=1}^{n}\sum_{j=1}^{m}\gamma_{\Lambda ij}\sum_{h=1}^{n}\left(k_{ih}\phi_{hj} + c_{ih}\phi_{hj}\lambda_j + m_{ih}\phi_{hj}\lambda_j^2\right) \\ & + 2\sum_{i=1}^{n}\sum_{j=1}^{m}\bar{\gamma}_{\Lambda ij}\sum_{h=1}^{n}\left(k_{ih}\bar{\phi}_{hj} + c_{ih}\bar{\phi}_{hj}\bar{\lambda}_j + m_{ih}\bar{\phi}_{hj}\bar{\lambda}_j^2\right) \end{aligned} \quad (4)$$

Received Aug. 5, 1997; revision received Nov. 18, 1997; accepted for publication Nov. 20, 1997.

*Senior Lecturer, Department of Mechanical Engineering.

†Director, Center for Intelligent Material Systems and Structures. Associate Fellow AIAA.

‡Graduate Research Assistant, Center for Intelligent Material Systems and Structures.